JES Focus Issue on Oxygen Reduction and Evolution Reactions for High Temperature Energy Conversion and Storage

Oxygen Reduction, Transport and Separation in Low Silver Content Scandia-Stabilized Zirconia Composites

E Ruiz-Trejo,[z] A. Bertei, A. Maserati, P. Boldrin, and N. P. Brandon

Department of Earth Science and Engineering, Imperial College, London SW7 2AZ, United Kingdom

Dense composites of silver and Sc-stabilized ZrO_2 (Ag-ScSZ) are manufactured from ScSZ sub-micrometric particles coated with silver using Tollens' reagent. A composite with 8.6 vol % of silver exhibits metallic conductivity of 186 S cm^{-1} and oxygen flux of 0.014 μmol cm^{-2} s^{-1} at 600°C for a 1-mm thick membrane when used as a pressure-driven separation membrane between air and argon. To gain insight into the role of oxygen transport in Ag and ScSZ, a dense non-percolating sample (Ag 4.7 vol%) is analyzed by impedance spectroscopy and the transport of oxygen through both phases is modelled. Oxygen transport takes place in both silver and ScSZ but it is still dominated by transport in the ionic conductor and therefore a large volume fraction of the ion conductor is beneficial for the separation. The oxygen transport in the silver clusters inside the composite is dominated by diffusion of neutral species and not by the charge transfer reaction at the interface between ScSZ and Ag, yet small silver particles on the surface improve the reduction of oxygen. Oxygen reduction is highly promoted by silver on the surface and there are no limitations of charge transfer at the interface between silver and ScSZ.

© The Author(s) 2017. Published by ECS. This is an open access article distributed under the terms of the Creative Commons Attribution 4.0 License (CC BY, http://creativecommons.org/licenses/by/4.0/), which permits unrestricted reuse of the work in any medium, provided the original work is properly cited. [DOI: 10.1149/2.0081710jes] All rights reserved.

Manuscript submitted March 21, 2017; revised manuscript received May 26, 2017. Published June 28, 2017. *This paper is part of the JES Focus Issue on Oxygen Reduction and Evolution Reactions for High Temperature Energy Conversion and Storage.*

The capability of metallic silver to reduce oxygen has been long known and recorded since Lucas reported it to Dalton as early as 1818[1] but better understood and quantified over the last 50 years.[2,3] This particular capability of silver can be exploited to incorporate oxygen into a solid system, be it a solid oxide fuel cell cathode[4] or an oxygen separation membrane.[5] Oxygen can be separated from air using a double phase membrane with an oxygen-ion conductor, e.g. scandia stabilized zirconia, and an electronic conductor, such as silver, that acts as a very efficient oxygen reducing agent. Scandia stabilized zirconia is known to have higher conductivity than yttria stabilized zirconia since it was first reported in 1900 by Nernst[6] but identified as an oxygen ion conductor by Wagner[7] several decades later. The use of double-phase metal ceramic composites to separate oxygen from air was first described by Mazanec,[8] who mixed Pd or Pt with YSZ and used the composite to drive chemical reactions. Although feasible, this approach normally requires large amounts of expensive metal to achieve percolation, ranging from 30 to 50 vol %, so that composite membranes cannot compete with the high oxygen flux reported in single phase perovskites, such as those reported by Teraoka[9] in 1985. To date, most of the research in high temperature oxygen separation is still performed in mixed ionic electronic conductive perovskites ABO_3, where A is one or more lanthanides and/or alkaline earths and B one or more transition metal oxides, for example $La_{1-x}Sr_xCo_{1-y}Fe_yO_{3-\delta}$ (LSCF)[9] or $Ba_{0.5}Sr_{0.5}Co_{0.8}Fe_{0.2}O_{3-\delta}$ (BSCF).[10] Nonetheless, these materials have two persistent problems: the high operating temperatures (>800°C) and the unsatisfactory chemical and mechanical stability in operating conditions. Furthermore, the chemical composition of the material affects both the stability and the oxygen separation capability, thus constraining the optimization of these functions and often resulting in an unsatisfactory compromise. Therefore, the double-phase approach is gaining interest again as it gives more flexibility to tailor the choice of conducting materials and their microstructure, as recently reported through the use of two conductive ceramic materials -an ionic one and an electronic one- such as $Ce_{0.9}Gd_{0.1}O_{2-x}$/LSCF[11] and Ag/$Ce_{0.9}Gd_{0.1}O_{2-x}$.[5] Especially, it has been shown that low levels of Ag can yield the necessary percolation for operation well below the 30–40 vol % usually considered as indispensable to achieve percolation.[12,13]

In this paper, reduction of oxygen, oxygen transport and separation in the intermediate temperature regime is demonstrated in a composite membrane of scandia-stabilized zirconia (ScSZ) and silver. Although currently scandia is a relatively expensive material, ScSZ's growing use as electrolyte in solid oxide fuel cells may lower its price.[14] The use of Tollens' reagent to fabricate metal ceramic composites for a variety of purposes has been reported recently in applications such as oxygen separation,[5] methane reforming,[15] hydrogen separation,[16] magnetic refrigeration[17] and anode fabrication.[18,19] In this work, the composite membrane fabrication is presented in detail that allows reproducibility and it is followed by characterization by SEM, XRD and conductivity tests. Then, two main samples are characterized in detail: 1.- a percolating sample is used as a separation membrane to unequivocally prove the reduction and separation of oxygen from air and the presence of silver percolation with a low metal content and 2.- a non percolating sample is studied by impedance spectroscopy and an electrochemical model is presented to provide for the first time an invaluable insight into the nature of the oxygen reduction and transport within silver and ScSZ.

Methods

Experimental.—*Manufacture.*—Sc-stabilized zirconia with stoichiometry $(Sc_2O_3)_{0.1}(ZrO_2)_{0.9}$ (labelled ScSZ) from Fuel Cell Materials was used as the starting powder. There were three initial nominal compositions: a nominally pure ScSZ, a composite with 10 wt% Ag, and one with 20 wt% Ag. The ScSZ particles were suspended in water and coated with silver using Tollens' reagent[16,20] as follows. A few drops of concentrated NH_4OH (27–30%) were added to 30 ml of $AgNO_3$ (0.1 M) resulting in a precipitate which was then cleared by adding more drops of ammonia (approximately 40 drops in total). This was followed by addition of 15 ml of KOH (0.80 M); if a precipitate was observed more drops of NH_4OH were added; the corresponding amount of sub-micrometric ScSZ (surface area of 8.9 m^2 g^{-1}) was then suspended in the clear solution using an ultrasonic bath for 20 minutes. Finally, silver was precipitated by adding drop-wise 3 ml of dextrose (0.25 M) as the reducing agent under continuous stirring. After 5 minutes of reaction the precipitate was then rinsed with deionized water and centrifuged (4000 rpm, 10–60 mins) to eliminate the remaining salts. This cleaning procedure was repeated five times. The precipitate was dried at 200°C for 1 h and then pelletized and isostatically pressed at 265 MPa for 1 minute. The pellets were fired in air at 1200°C or 1300°C for two hours using a heating/cooling rate of 5°C min^{-1}. The pellets were covered tightly with yttria stabilized zirconia (YSZ) powder to minimize silver losses during sintering. After

[z]E-mail: eruiztre@imperial.ac.uk

Downloaded on 2017-11-09 to IP 155.198.98.217 address. Redistribution subject to ECS terms of use (see ecsdl.org/site/terms_use) unless CC License in place (see abstract).

sintering, the surface of the sintered pellets was polished to homogenize the surface by eliminating YSZ and exuded silver. A nominally pure ScSZ dense sample was obtained by sintering at 1300°C for one hour.

Structural and electrical characterization.—A field emission gun scanning electron microscope (FEG-SEM Gemini 1525) was used for imaging of the materials. Images of fracture surfaces of the membranes were collected to confirm the dense nature of the samples. The chemical composition was analyzed with EDX using a Phenom ProX SEM microscope. The powders and consolidated samples were analyzed with an X'Pert PRO MRD X-ray diffraction system. The density and open porosity was measured with the Archimedes' method using deionized water as the immersion fluid after previously boiling the samples for one hour to ensure all air bubbles were eliminated. The volume of the open porosity is obtained from the weight difference between a dry sample and a soaked sample.

Conductivity.—Initial screening between percolating and non-percolating samples was achieved with a hand-held ohmmeter or a simple metal detector. The conductivity of a percolating sample was then measured using the van der Pauw technique between room temperature and 600°C. The linearity of the relationship between measured current and voltage was tested at different temperatures by passing different currents (from ± 5 mA to ± 250 mA). Four platinum tips were used to connect the disc-shaped sample with a potentiostat (Autolab PGSTAT302).

This was also used for measuring electrochemical impedance spectroscopy (EIS) in a nominally pure ScSZ and a non-percolating Ag-ScSZ composite; both samples were tested in air within the range of temperatures 600–800°C. The EIS response was measured in the frequency range 0.1 Hz–1 MHz and a potential of a 20 mV with silver paint as electrodes.

Permeation.—A pellet of the percolating Ag-ScSZ composite with a surface area of 2.54 cm^2 and thickness of 1 mm was attached at the end of an alumina tube and sealed with an alumina-based inorganic adhesive (Aron ceramics D), so that one side of the pellet was exposed to a flow of air, while the inner side of the alumina tube could be swept with argon. This set-up was placed into a furnace and tested between 500°C–600°C after curing of the sealant. The air was fed at 130 mL min^{-1} at Normal Temperature and Pressure (NTP) while the inner side was swept with zero-grade argon at 100 mL min^{-1}. Immediately prior to the permeation experiment a mass spectrometer downstream was calibrated with a mixture of 1% nitrogen in argon and a mixture of 2% of oxygen in argon, both supplied by BOC. During the experiments the mass to charge ratio (m/e) signals of nitrogen and oxygen were followed. During data analysis, it was assumed that any nitrogen present in the sweep gas mixture came from leaks from air. By measuring the amount of nitrogen present it was possible to calculate the oxygen present due to unwanted leaks and subtract this from the measured oxygen concentration in the sweep gas mixture.

Modelling.—The impedance of ScSZ and non-percolating Ag-ScSZ composite was interpreted according to the following mechanistic equivalent circuit.

The normalized impedance Z_{cell} of the cell Ag|Ag-ScSZ|Ag is given by the impedance of the non-percolating composite Ag-ScSZ Z_{ey} in series with the impedance of the two silver electrodes Z_{ed}:

$$Z_{cell} = Z_{ey} + 2 \cdot Z_{ed} \quad [1]$$

The impedance of the Ag-ScSZ composite Z_{ey} is calculated as

$$Z_{ey} = \frac{L_{ey}}{\sigma_{ey}} \quad [2]$$

where L_{ey} is the sample thickness and σ_{ey} is the complex conductivity. For the composite, σ_{ey} is calculated according to the Maxwell-Wagner model with ScSZ as the continuous phase and silver as non-percolating phase:[21]

$$\sigma_{ey} = \sigma_{ScSZ} \frac{2\sigma_{ScSZ} + \sigma_{Ag} - 2\phi_{Ag}\left(\sigma_{ScSZ} - \sigma_{Ag}\right)}{2\sigma_{ScSZ} + \sigma_{Ag} + \phi_{Ag}\left(\sigma_{ScSZ} - \sigma_{Ag}\right)} \quad [3]$$

where σ_{ScSZ} is the ionic conductivity of ScSZ, σ_{Ag} the complex conductivity due to oxygen atom diffusion within silver droplets and ϕ_{Ag} the volume fraction of silver in the Ag-ScSZ composite. For the pure ScSZ, $\sigma_{ey} = \sigma_{ScSZ}$ as $\phi_{Ag} = 0$.

The complex conductivity due to oxygen atom diffusion within silver droplets (σ_{Ag}) is calculated according to a non-uniform diffusion element, similarly to that used in the electrode (see after), as follows:

$$\sigma_{Ag} = \frac{L_{Ag}}{Z_{Ag}} \quad [4]$$

with:

$$Z_{Ag} = \frac{RT}{4^2F^2} \frac{1}{C_O\sqrt{D}} \frac{\tanh\left(\frac{L_{Ag}}{\sqrt{D}}(i\omega)^{p_{Ag}}\right)}{(i\omega)^{p_{Ag}}} \quad [5]$$

where C_O and D represent the solubility and diffusion coefficient of oxygen atoms in silver, L_{Ag} is the characteristic length of silver droplets in the Ag-ScSZ composite while the exponent p_{Ag} takes into account the non-uniformity of diffusion within a silver droplet. D is assumed to be independent of oxygen concentration and C_O is considered spatially uniform (i.e., no oxygen gradients) because impedance is collected at open-circuit equilibrium. All the parameters are determined by fitting of impedance spectra, C_O and D are compared with literature values afterwards. Additionally, i is the imaginary unit, ω is the angular frequency, T is the absolute temperature while R and F represent the gas and Faraday constants, respectively.

The impedance response of the Ag electrode Z_{ed} is given by two contributions (see[4] and Figure 1):

1. adsorption of molecular oxygen, dissociation in oxygen atoms and incorporation into the silver bulk:

$$O_{2(g)} \rightarrow 2O_{(Ag)} \quad [6]$$

which is represented by a ZARC element as follows:

$$Z_{ZARC} = \left(\frac{1}{R_1} + \frac{1}{\sigma_{CPE}(i\omega)^{\alpha}}\right)^{-1} \quad [7]$$

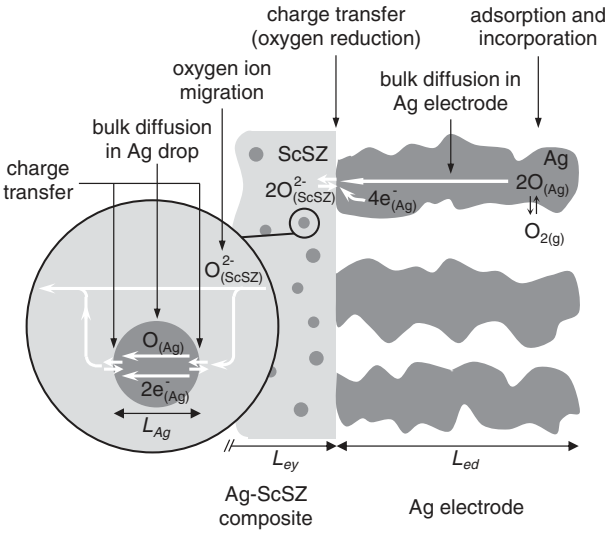

Figure 1. Schematic representation of the transport and electrochemical processes occurring in non-percolating samples Ag|Ag-ScSZ|Ag as considered by the model.

Downloaded on 2017-11-09 to IP 155.198.98.217 address. Redistribution subject to ECS terms of use (see ecsdl.org/site/terms_use) unless CC License in place (see abstract).

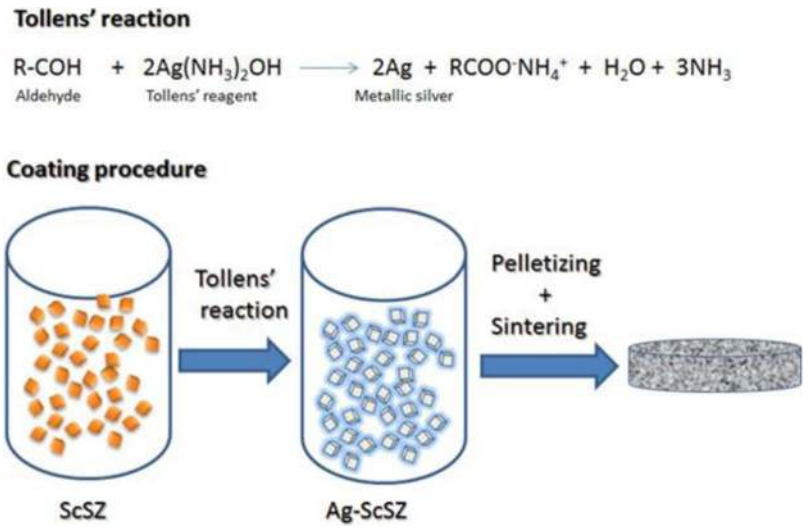

Figure 2. Schematic representation of the fabrication process. The aldehyde represented corresponds to the species in equilibrium with the dextrose used.

where R_1 is the resistance of the adsorption and incorporation process (Eq. 6), σ_{CPE} is the time constant of the constant phase element (CPE) and α is the exponent, with $-1 < \alpha < 0$.

2. bulk diffusion of oxygen atoms along the thickness of the Ag electrode, represented by a Non-Uniform Diffusion (NUD) element:

$$Z_{NUD} = \frac{RT}{4^2F^2}\frac{1}{C_O\sqrt{k_{eff}D}}\frac{\tanh\left(\frac{L_{ed}}{\sqrt{k_{eff}D}}(i\omega)^{p_{ed}}\right)}{(i\omega)^{p_{ed}}} \quad [8]$$

where L_{ed} is the electrode thickness and k_{eff} is the dimensionless effective solid diffusivity factor, which takes into account the solid volume fraction and tortuosity of the electrode according to the Bruggeman correlation.[22] Note that Eqs. 5 and 8 are similar because they represent the same non-uniform diffusion process of oxygen atoms within silver droplets and silver electrode, respectively. The intrinsic values of oxygen solubility C_O and diffusivity D are the same in both the silver droplets (Eq. 5) and the electrode (Eq. 8), while the characteristic lengths L_{Ag} and L_{ed} as well as the exponents p_{Ag} and p_{ed} differ due to the different geometric and microstructural characteristics of silver droplets and silver electrode.

The silver electrodes and the samples tested have an interface where oxygen atoms from Ag are reduced to oxygen ions in ScSZ (see Figure 1). This is represented by the charge transfer oxygen reduction reaction:

$$O_{(Ag)} + 2e^-_{(Ag)} \leftrightarrow O^{2-}_{(ScSZ)} \quad [9]$$

This reaction is considered to be fast enough to be at pseudo-equilibrium and consequently does not produce a detectable impedance contribution.[4]

Results and Discussion

Manufacture and structural characterization.—A summary of the manufacturing process is depicted in Figure 2 including the reaction of coating. ScSZ is a white powder that upon coating with silver turns to a purple/brown color.

Figure 3 shows SEM images of the uncoated and Ag-coated ScSZ with two different initial contents of silver. The ScSZ particles match the diameter of 119 nm expected from the surface area of the powder (8.9 $m^2\ g^{-1}$); the coated particles seem to retain the same morphology and the particle size barely changes. As no clear agglomeration of silver is observed, it is assumed that the particles of ScSZ are coated uniformly: for Ag-ScSZ a silver layer of 1 nm is expected for 10 wt% Ag and 2 nm for 20 wt% Ag.

A variety of sintering conditions were tested trying to achieve metallic conductivity and low porosity using two initial silver contents (10 wt% and 20 wt%). In general, sintering temperatures of 1100°C and below did not achieve high density although they were percolating. The best conditions to achieve low porosity and percolation of the silver were 1200°C for 2 hours. Table I summarizes the properties of the consolidated samples. The coated samples lost silver after deposition and sintering at high temperatures. It must be said that the conditions of the manufacturing are not yet optimized. Two samples, a percolating and a non-percolating one, were used in the following experiments.

Figure 4 shows the microstructure of three samples after sintering. Pristine ScSZ is very dense, while there is some porosity in the silver composites. Although the FEG-SEM gives an insight into the nature of the porosity, silver and ScSZ cannot be distinguished. Instead, EDX analysis was used to identify the two phases and the quantification is presented in Table I. Figure 5 shows the back scattered electron image as well as the EDX energy spectrum for the percolating sample (8.6 vol % Ag). The distribution and dimensions of the silver grains are completely different to the distribution of Ag–ceramic composites obtained by mixing Ag or Ag_2O powder with ceramics.[13] Not only is the grain size considerably smaller but also Figure 5 shows a constellation of interconnected silver grains rather than isolated islands. However, no quantification can be drawn from this picture as the presence of small grains of silver further complicates a full map of silver as in our previous work on Gd-doped ceria-Ag composites.[5]

Figure 6 shows the XRD pattern of ScSZ and Ag-ScSZ composites at room temperature: as expected there was no reaction between them or oxidation of silver at high temperature; the pattern shows that ScSZ is a mixture of cubic and rhombohedral phases as a consequence of the high temperature treatment: it is known that ScSZ evolve into different phases depending upon composition and anneal temperature and time.[23–25] The silver melting point is 953°C and its high volatility is known, however, even after sintering at 1300°C, silver was retained in the composite, probably due to the fast densification of ScSZ trapping the silver in the ceramic matrix. Two conditions seem necessary to obtain a percolating structure with a low content of metal: i) an onset of sintering temperature low enough to minimize silver losses and ii) a silver content in the range 5–10 vol %.

Conductivity and permeation.—Figure 7 shows the conductivity as a function of temperature for ScSZ, non-percolating Ag-ScSZ (4.7 vol % Ag) and percolating Ag-ScSZ (8.6 vol % Ag) as well as reference data for ScSZ and silver. The ScSZ values match well those of previous reports.[25–27] The dc conductivity of the non-percolating Ag-ScSZ was obtained from fitting impedance data of the sample as described in the modelling section and corresponds to both oxygen

Downloaded on 2017-11-09 to IP 155.198.98.217 address. Redistribution subject to ECS terms of use (see ecsdl.org/site/terms_use) unless CC License in place (see abstract).

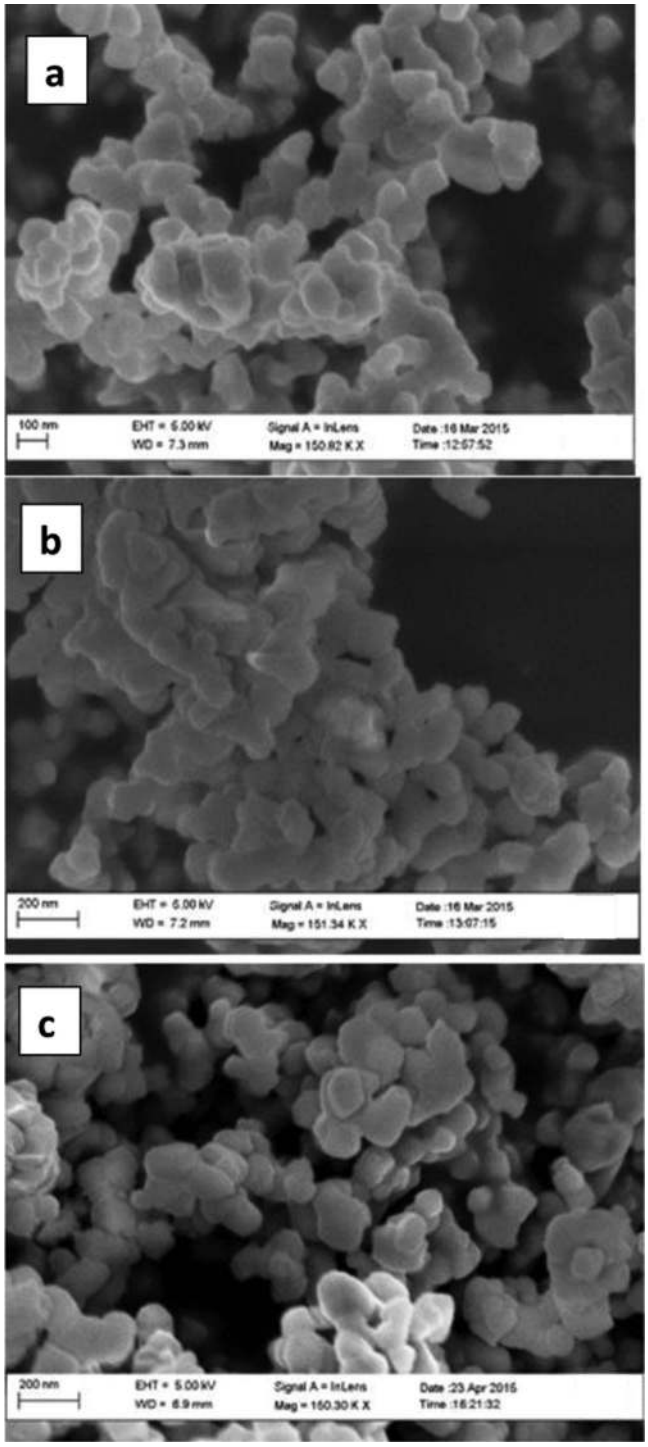

Figure 3. a) Pristine ScSZ powders b) Ag-ScSZ powder (10 wt% Ag) and c) Ag-ScSZ powder (20 wt% Ag).

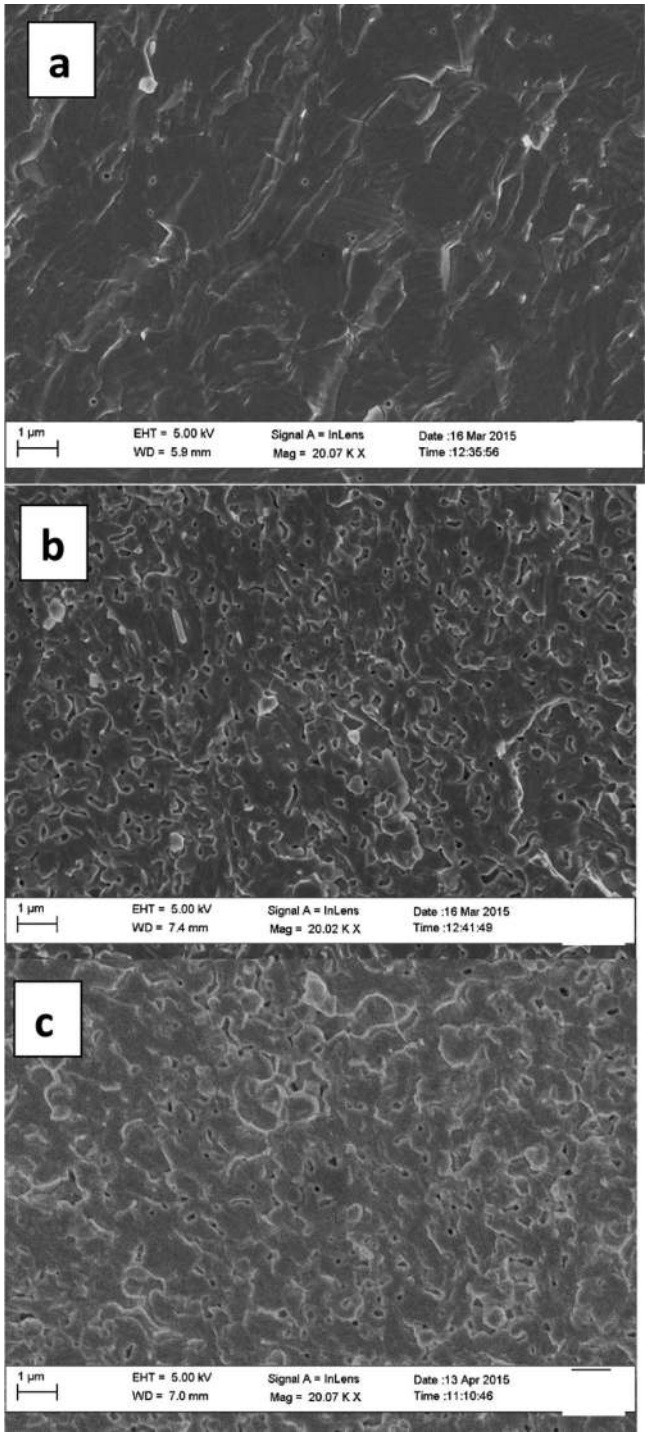

Figure 4. Micrograph of fracture surfaces of a) ScSZ sintered at 1300°C, b) Ag-ScSZ sintered at 1200°C, 4.7 vol % Ag, c) Ag-ScSZ sintered at 1200°C, 8.6 vol % Ag.

Table I. Sintering conditions and resulting properties of pristine ScSZ and Ag-ScSZ composites.

Sintering T (°C), time	Ag wt% EDX	Ag vol% EDX	Density expected (based on EDX data) g mL^{-1}	Archimedes' density g mL^{-1}	Theoretical density %	Open porosity %	Percolation
1300, 2h	0	0	5.68	5.61	98.8	0.5	No
1300, 2h	7.7	4.3	5.89	5.53	93.9	1.2	No
1200, 2h	8.4	4.7	5.91	5.73	96.9	0.8	No
1200, 2h	14.8	8.6	6.09	5.90	96.9	2.9	Yes

Downloaded on 2017-11-09 to IP 155.198.98.217 address. Redistribution subject to ECS terms of use (see ecsdl.org/site/terms_use) unless CC License in place (see abstract).

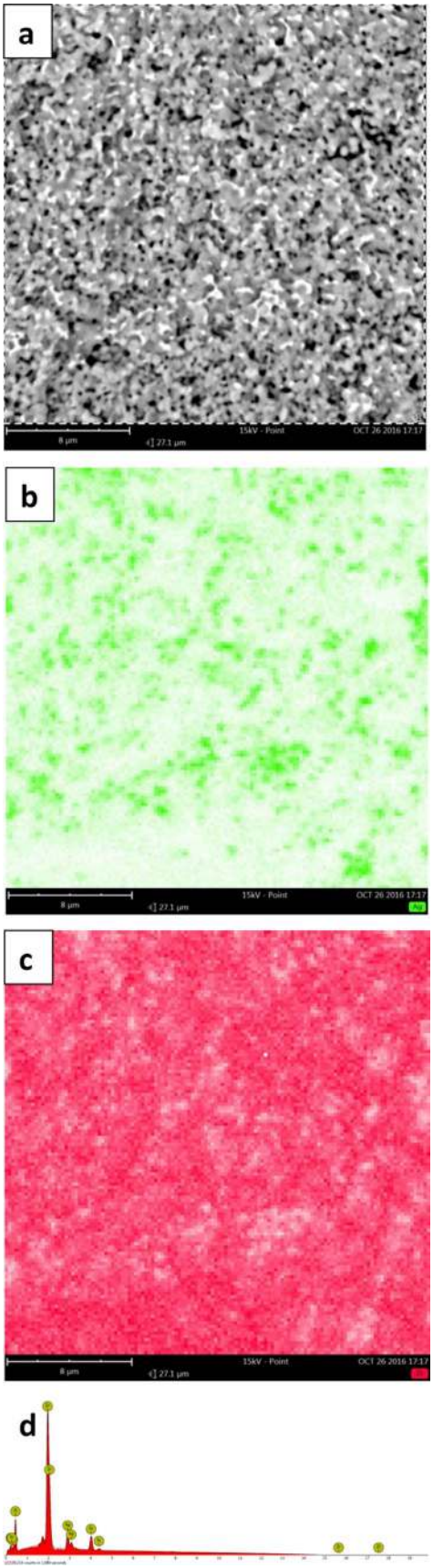

Figure 5. EDX analysis of silver on a percolating sample (8.6 vol % Ag). a) Back scattered image, b) EDX map of silver (silver in green), c) EDX map of zirconium (in red), d) Energy spectrum of the sample. Note that the contrast in the back scattered image has been increased to improve the visibility of silver.

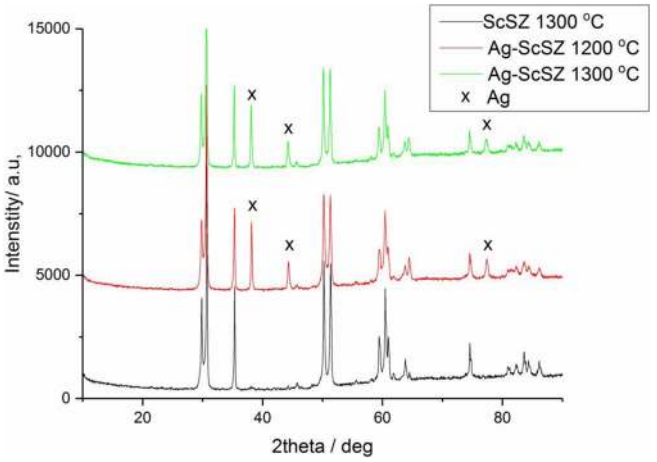

Figure 6. XRD pattern of ScSZ sintered at 1300°C and Ag/ScSZ sintered at 1200°C and 1300°C.

transport in ScSZ as well as in the silver clusters embedded into the ScSZ matrix. The oxygen flux corresponds almost exclusively to the transport of oxygen ions through ScSZ.

The dc conductivity of the percolating Ag-ScSZ composite unequivocally shows metallic behavior with a temperature coefficient equal to 1.87×10^{-3} K^{-1} comparable to 4.1×10^{-3} K^{-1} in pure silver,[28] indicating that the electrical transport is dominated by percolating silver despite its low content (8.6 vol %), a content well below 40% vol necessary when manufacturing with conventional solid state mixtures.[13,14] A few interesting experimental observations during the measurements in percolating Ag-ScSZ composite were that below 400°C, upon imposing a dc current, the system achieved a stable voltage within a minute, however, at temperatures above 400°C, the measurements were considerably noisier, i.e. when imposing a current through the pellet the voltage was relatively unstable. The sample was left to equilibrate for at least 10 minutes, but even in these cases the measurement was noisy. There are several phenomena that can account for this observation. As studied in Impedance of non-percolating Ag-ScSZ and ScSZ section, oxygen is reduced in both ScSZ and in silver, the dissolution of oxygen on one side of the membrane (cathode) and its evolution in the other side (anode) can cause a temporary change in the local resistance –and probably the temperature- at the contacts. After the dc experiment, silver droplets

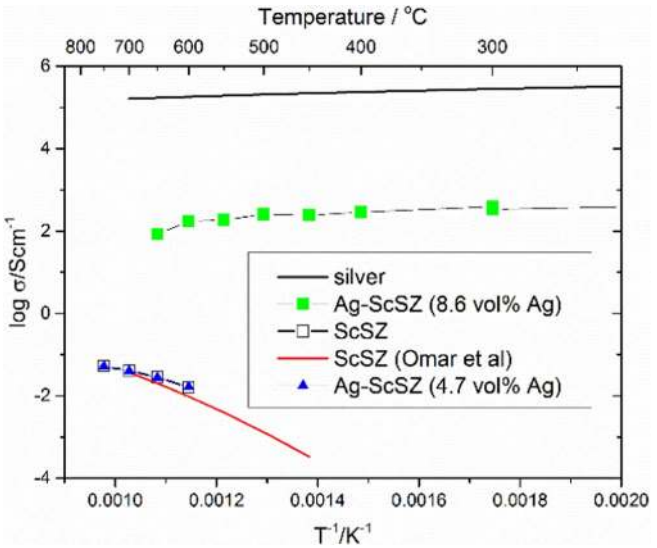

Figure 7. Conductivity of the composite Ag-ScSZ, ScSZ and literature data for silver and ScSZ.

Downloaded on 2017-11-09 to IP 155.198.98.217 address. Redistribution subject to ECS terms of use (see ecsdl.org/site/terms_use) unless CC License in place (see abstract).

were observed at the surface where the van der Pauw conductivity was measured but not on the opposite face, indicating the possibility of silver migration during the measurement. The phenomenon of electromigration, the migration of silver through a non-conductive surface, is known,[29] while the migration of ionic silver from metallic silver under a strong electric field has been reported in glass[30] and even in ScSZ.[31] In the latter study, a change in color from white to orange indicated the presence of silver mobility according to the authors but in the composites Ag-ScSZ no traces of orange color were observed. During the open-circuit impedance measurements of non-percolating samples there is no driving force for Ag electromigration, so the electrode and Ag-ScSZ composite microstructures are rather stable over time. The noisy signal measured during the dc studies may also be related to the transport of charged species in the bulk since above 450°C the net migration of oxygen becomes considerable and the transport of electrons and the transport of oxygen cannot be considered independent anymore, i.e. the oxygen transport seems to affect the mobility of the electrons as the Onsager coefficients for transport are not independent.[32]

In the range 500°C–600°C the electronic conductivity is more than three orders of magnitude higher than the ionic conductivity in nominally pure ScSZ. Previous experimental and theoretical studies on metal-ceramic composites prepared by conventional ceramic processing established 30–40 vol% as the minimum amount of metal to provide percolation[12,13,33–35] but here that limit has been driven to lower metal contents by using an innovative processing route. In this case, the electronic percolation can theoretically take place along the surface of ScSZ grains, thus requiring less Ag to achieve percolation. This has a parallel in infiltrated electrodes for solid oxide fuel cell applications, wherein the formation of a surface layer of metallic phase can result in a percolation threshold as low as 5.3 vol %,[5,36] depending on the thickness and homogeneous distribution of the metallic coating layer. Therefore, the large amounts of metal needed for percolation used at the early stages of research into metal ceramic composites are not needed anymore. Percolation can be achieved with silver with contents below 10 vol % as shown for Ag and doped ceria and Ag-ScSZ in this work.[5,15]

A permeation experiment was carried out to confirm the separation of oxygen from air at intermediate temperatures. The concentrations of N_2 and O_2 were measured by mass spectrometry, with the nitrogen content being used to measure the amount of air leaking into the system. The unwanted leak of oxygen was then subtracted from the total O_2 measured in the sweep gas leading to the oxygen flux across the membrane. The leaks are most likely due to the sealing since even after boiling the samples for 1 hour in the Archimedes method, the open porosity was only 2.9 vol%, below the percolation threshold of the pore phase, equal to 4 vol%.[37,38]

Figure 8 shows the oxygen permeance between 550°C and 600°C, the inset shows the raw data including the N_2 signal to show the unequivocal separation from air. The theoretical upper bound of the oxygen flux is calculated with Wagner's theory:

$$J_{O_2} = \frac{RT}{4^2 F^2 L} \sigma^{eff}_{ScSZ} \ln \frac{p'_{O_2}}{p''_{O_2}} \qquad [10]$$

where $L = 1$ mm is the membrane thickness and σ^{eff}_{ScSZ} is the effective ionic conductivity of ScSZ in the membrane, which is calculated by multiplying the bulk ionic conductivity of ScSZ according to Table II and the effective conductivity factor according to the Hashin-Shtrikman upper bound[39,40] $\gamma_{eff} = (1-\phi_{Ag}-\phi_{pore})/(1+(\phi_{Ag}+\phi_{pore})/2) = 0.837$ for $\phi_{Ag} = 8.6\%$ and $\phi_{pore} = 2.9\%$. In Eq. 10, p'_{O_2} is the partial pressure of oxygen in the air side, equal to 0.21 atm, while p''_{O_2} is the partial pressure of oxygen in the sweep side as measured by mass spectrometry. Although the equation is a simplification of the permeation process, it can be used as a reference upper bound for the experimental values. Incidentally, the use of Eq. 10 is justified by the modelling section since, as reported in the next section, ionic conduction is the rate-determining transport process in the membrane.

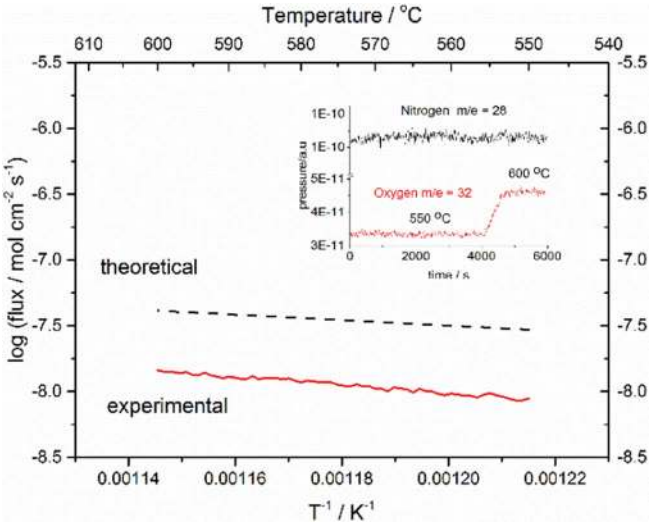

Figure 8. Permeance of oxygen for a 1-mm thick Ag-ScSZ (8.6 vol % Ag) under a gradient of argon and air. The inset shows the raw data. The surfaces are active for oxygen reduction.

The calculated and measured values for the oxygen permeation flux between 550°C and 600°C are presented and show a good consistency considering the large number of variables that can affect the theoretical value. It is also worth noting that the surface of the samples did not need any treatment or coating as silver acts effectively as oxygen reducing agent and, as in the case of Gd-doped ceria, the presence of silver increases the oxygen surface exchange coefficient.[5] An oxygen flux of 0.014 μmol cm^{-2} s^{-1} at 600°C for a 1-mm thick membrane was achieved.

At temperatures above 600°C the sealing was compromised and after the permeation experiment was finished it was observed that the silver formed a dendritic growth at the edge of the seal in the low p_{O_2} side. This might be an indication that silver migrates during operation at high temperatures under a chemical potential gradient; similar examples can be found in the literature: for example, in the system Ag–SnO_2–In_2O_3, exudation of silver was observed as a consequence of the chemical potential gradient and not as a consequence of the internal stresses during oxidation. Silver exudation has been found to occur always in the direction opposite to the oxygen concentration gradient.[15,41] The development of oxygen separation membranes will require sealing issues and the migration of silver to be addressed along with the manufacturing of thinner membranes to achieve a higher oxygen flux.

Impedance of non-percolating Ag-ScSZ and ScSZ.—The model presented above was used to interpret the impedance spectra at different temperatures of two non-percolating samples: Ag|ScSZ|Ag, made with a pure ScSZ electrolyte, and Ag|Ag-ScSZ|Ag, which contains non-percolating silver (4.7 vol%). In both the cases, the thickness of the samples was $L_{ey} = 1.95$ mm and the thickness of the electrode was roughly estimated to be as $L_{ed} = 3.2$ μm from SEM micrographs. Based on the estimated electrode porosity, k_{eff} was taken equal to 0.5 according to the Bruggeman correlation.[22]

Table II. Ionic conductivity of ScSZ, σ_{ScSZ}, resulting from the fitting of the ohmic resistance of Ag|ScSZ|Ag.

T°C	σ_{ScSZ} S m^{-1}
600	1.786
650	3.018
700	4.370
750	5.617
800	6.604

Downloaded on 2017-11-09 to IP 155.198.98.217 address. Redistribution subject to ECS terms of use (see ecsdl.org/site/terms_use) unless CC License in place (see abstract).

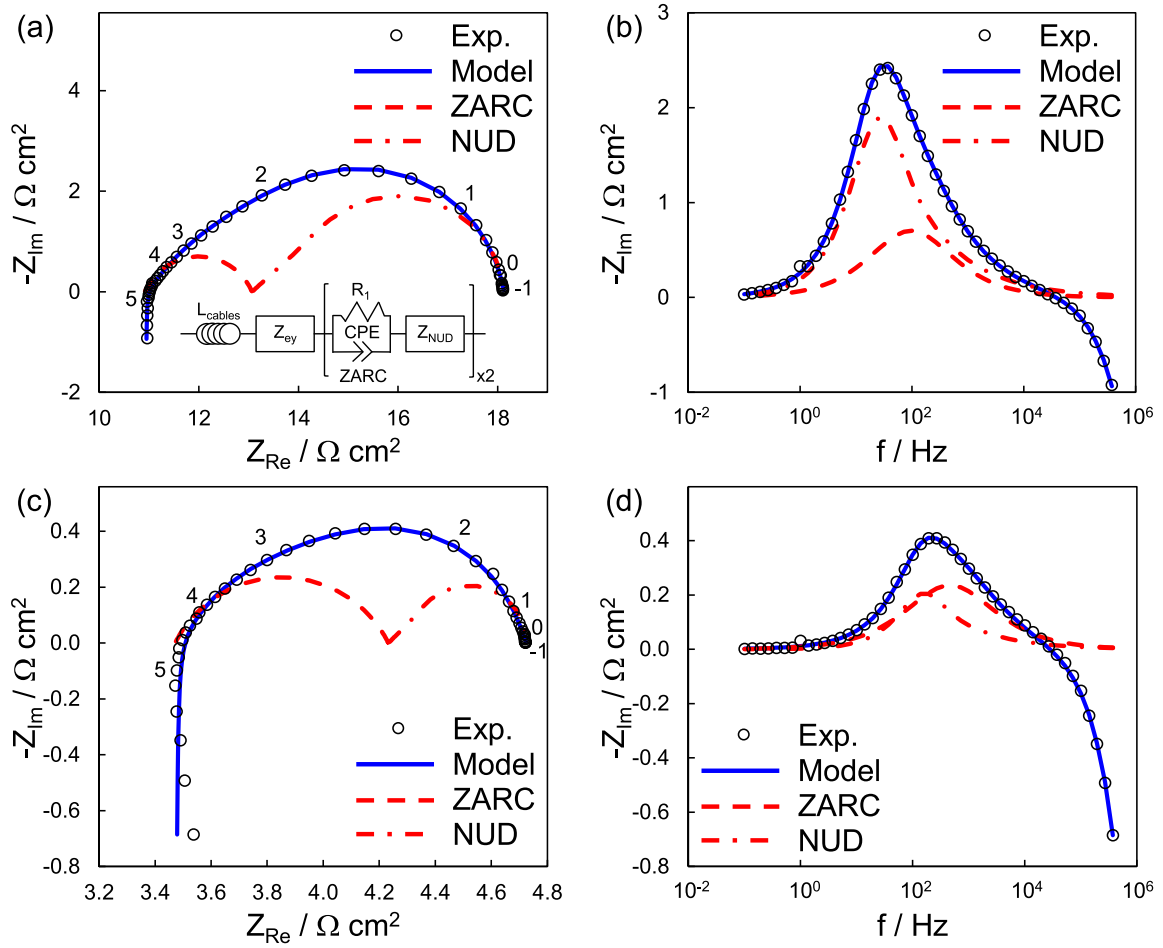

Figure 9. Fitting of Ag|ScSZ|Ag at 600°C (a and b) and at 750°C (c and d) according to the model presented. The numbers next to the data points correspond to the log of the frequency. The inset in a) shows the equivalent circuit used for the fitting.

Analysis of sample Ag|ScSZ|Ag and ScSZ conductivity.—The bulk of this sample does not contain silver, thus $\phi_{Ag} = 0$. In such a case, the impedance of the electrolyte becomes a pure resistance equal to $Z_{ey} = R_{ey} = L_{ey}/\sigma_{ScSZ}$. Thus, the fitting of spectra at different temperatures is useful to determine the ionic conductivity σ_{ScSZ} as a function of temperature from the high-frequency intercept R_{ey}, as reported in Table II. From the same data fitting, the adsorption and diffusion of oxygen atoms in the silver electrodes was obtained similarly to van Herle and McEvoy.[4] All fitted parameters are reported in the annex (Table AI).

The fitting of the EIS spectra was performed using ZView and an inductive element was added in series to account for the cable inductance. Figure 9 shows the fitting of the spectra at two different temperatures. The different contributions to impedance are also reported: NUD refers to Z_{NUD} (Eq. 8), ZARC to Z_{ZARC} (Eq. 7) and Z_{ey} to the electrolyte impedance which is a pure resistance in this sample.

Table II reports the values of ScSZ ionic conductivity σ_{ScSZ} fitted from the high-frequency intercept Z_{ey} at each temperature. These values are compared in Figure 10 with expected values according to the following correlations provided in the literature:[27,42]

$$\sigma_{ScSZ} = \frac{100}{T} 10^{\left(3.34 + 1.51\frac{1000}{T} - 3.16\left(\frac{1000}{T}\right)^2\right)} \left[\mathrm{S\,m^{-1}}\right] \quad [11]$$

$$\sigma_{ScSZ} = 6.5 \cdot 10^4 \exp\left(-\frac{9250}{T}\right) \quad \left[\mathrm{S\,m^{-1}}\right] \quad [12]$$

The analysis of results shows that the model reproduces the experimental data across the whole frequency range for all temperatures, and decouples the depressed electrode feature into two contributions as expected. In particular, the ionic conductivity of ScSZ, which is evaluated from fitting the electrolyte resistance $Z_{ey} = R_{ey}$, is fairly consistent with the values reported in the literature, as shown in Figure 10. Therefore, the values of σ_{ScSZ} can be considered acceptable and are used in the next section for interpreting the impedance spectra of Ag|Ag-ScSZ|Ag.

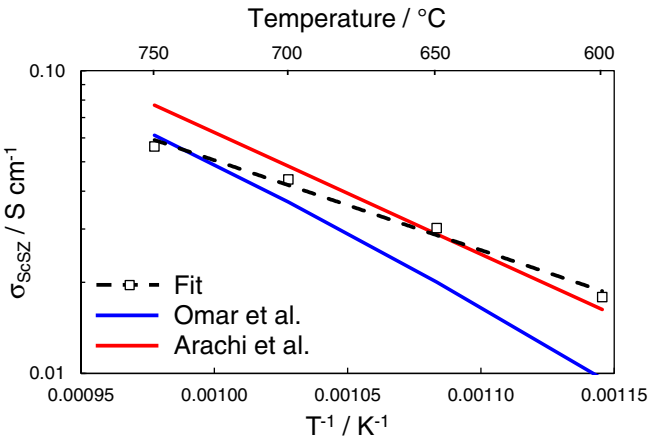

Figure 10. Arrhenius plot of the ScSZ ionic conductivity fitted in Ag|ScSZ|Ag (squares). Estimated values from the literature are reported with solid lines (Eq. 11 in blue, Eq. 12 in red). The activation energies are 0.59 eV, 0.95 eV and 0.80 eV for fitted results, Eq. 11 and Eq. 12, respectively.

Downloaded on 2017-11-09 to IP 155.198.98.217 address. Redistribution subject to ECS terms of use (see ecsdl.org/site/terms_use) unless CC License in place (see abstract).

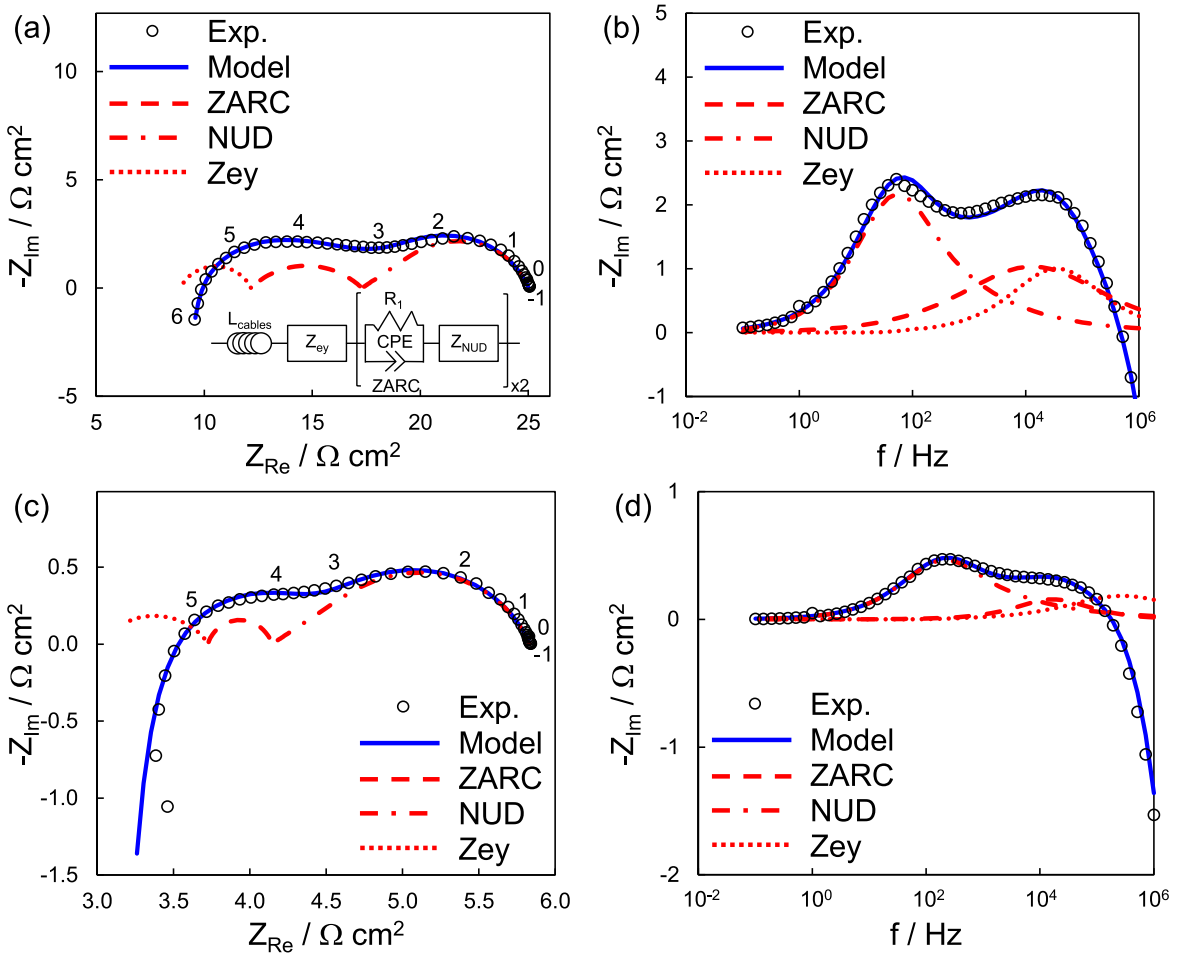

Figure 11. Fitting of Ag|Ag-ScSZ|Ag (4.7 vol % Ag) at 600°C (a and b) and at 750°C (c and d) according to the model presented.

Analysis of sample Ag|Ag-ScSZ|Ag and oxygen transport properties.—Figure 11 shows the experimental spectra of non-percolating Ag|Ag-ScSZ|Ag (4.7% vol Ag) for different temperatures. Comparing Figure 9 and Figure 11, there is clearly an extra element at high frequency in the impedance spectra of the Ag-ScSZ sample. The low/medium-frequency feature roughly matches the polarization response of Ag|ScSZ|Ag, which was ascribed to the silver electrodes. The additional depressed contribution at high frequency must then be associated with the processes occurring within the non-percolating Ag-ScSZ composite.

The application of the model allows for the fitting and deconvolution into different contributions. The corresponding fitting parameters are reported in Table III and plotted in Figure 12 along with the correlations reported in the literature[4] (see Eqs. 13 and 14). All fitted parameters are in the annex in Table AII. Note that σ_{ScSZ} is not re-fitted and the same values obtained in the Ag|ScSZ|Ag sample reported in Table II are used to describe the ion conduction in the ScSZ matrix: only the value at 600°C is adjusted to better fit the data. Notably, the same values of C_O and D are used in both the impedance element Z_{ey} of the Ag-ScSZ composite (Eqs. 2–5) and the NUD element of the electrode (Eq. 8).

Table III. Fitted parameters for Ag|Ag-ScSZ|Ag (4.7 vol % Ag). $k_{eff} = 0.5$ is used in the electrode.

T [°C]	D [$m^2\ s^{-1}$]	C_O [mol m^{-3}]	ϕ_{Ag}	L_{Ag} [μm]
600	$6.332 \cdot 10^{-10}$	1.275	0.0710	0.8
650	$9.789 \cdot 10^{-10}$	1.624	0.0473	0.8
700	$1.265 \cdot 10^{-9}$	2.266	0.0473	0.8
750	$1.608 \cdot 10^{-9}$	2.691	0.0473	0.8

$$C_O = 4.68179 \cdot 10^{(1.403-2593/T+0.5\log_{10}(p_{O_2}\cdot 760))} \left[\text{molm}^{-3}\right] \quad \text{with } pO_2 \text{ in atm} \qquad [13]$$

$$D = 4.9 \cdot 10^{-7} \exp\left(-\frac{0.503eV}{RT}\right) \left[\text{m}^2\text{s}^{-1}\right] \qquad [14]$$

Figure 11 shows that the model fits the experimental data reasonably well across the whole frequency range over the measured temperatures of 600–750°C. The contribution of the ZARC element to electrode polarization resistance, that is, the ratio between R_1 and the electrode resistance, lies between 20 and 40%, which is in good agreement with the range 25–30% found in Ref. 4 The activation energies of C_O (0.40 eV) and D (0.47 eV) match reasonably well those reported by van Herle and McEvoy, equal to 0.51 eV and 0.50 eV, respectively (see Figure 12). In addition, despite the fact that the values of k_{eff} and L_{ed} are only estimated, the fitted D and C_O lie within the same order of magnitude of the values obtained in Ag|ScSZ|Ag and are consistent with values reported in the literature, enabling acceptable fitting of both the electrode and composite Ag-ScSZ response by using the same values of D and C_O in both electrode (Eq. 8) and composite Ag-ScSZ (Eq. 5). In addition, except at 600°C, the same values of σ_{ScSZ} are used in both Ag|ScSZ|Ag and Ag|Ag-ScSZ|Ag

Downloaded on 2017-11-09 to IP 155.198.98.217 address. Redistribution subject to ECS terms of use (see ecsdl.org/site/terms_use) unless CC License in place (see abstract).

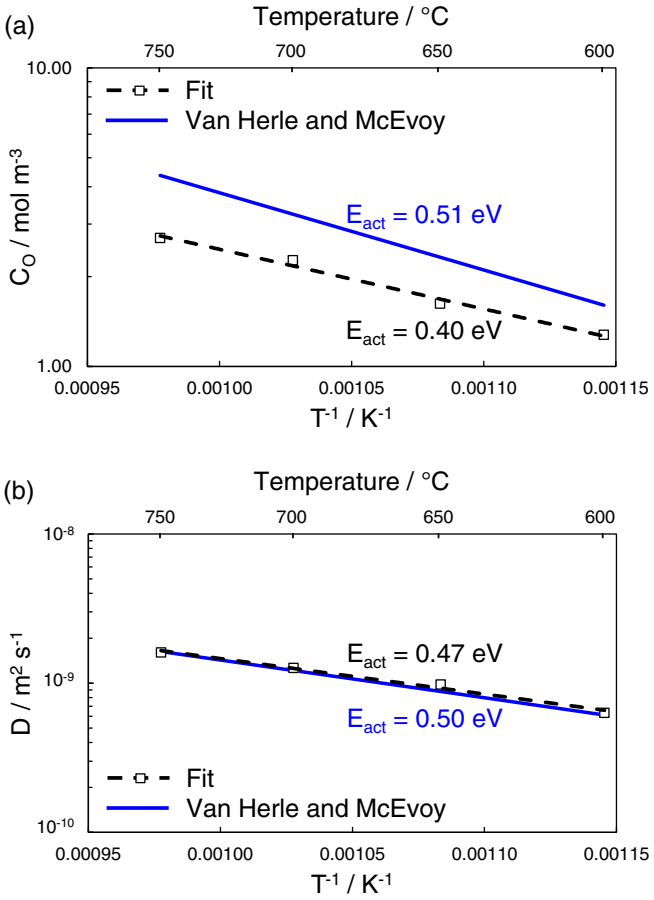

Figure 12. Arrhenius plot of the fitted parameters (squares) for non-percolating Ag|Ag-ScSZ|Ag (4.7 vol % Ag) in comparison with estimated values from Ref. 4 (solid lines): a) equilibrium concentration of oxygen in silver; b) diffusion coefficient of oxygen atoms in silver.

samples, showing that the ion conduction in the ScSZ matrix is coherently reproduced in both the samples. These results are positive confirmations of the validity of the model and the consistency of the experimental data of the Ag|Ag-ScSZ|Ag sample.

Notably, the model provides a mechanistic explanation of the high-frequency contribution present in this sample, which is due to the diffusion of oxygen atoms in the Ag drops dispersed within the Ag-ScSZ composite. Indeed, the fitting of the additional feature with the Maxwell-Wagner model (Eq. 3) is rather good. Nonetheless, while the characteristic length of Ag grains L_{Ag} remains constant with temperature, ϕ_{Ag} differs from the nominal value of 4.7 vol% (8.4 wt%) at 600°C. This inaccuracy may be attributed to the difficulty to deconvolve the Ag-ScSZ impedance contribution Z_{ey} from the middle-frequency electrode feature Z_{ZARC}, as they both appear in the same frequency range at 600°C (see Figure 11b), thus affecting the estimation of the specific parameters of the Ag-ScSZ composite response Z_{ey}, such as ϕ_{Ag}. However, it is remarkable that both the fitted L_{Ag} and ϕ_{Ag} assume credible values.

Therefore, despite the complexity of the system compared to Ag|ScSZ|Ag, the fitting of the electrode response provides specific parameters which are consistent with the literature. In addition, the additional feature present in the impedance of non-percolating Ag|Ag-ScSZ|Ag can be interpreted as a contribution from oxygen atom diffusion in the Ag grains, which is described with the same values of parameters D and C_O used to fit the electrode response, along with credible microstructural values of L_{Ag} and ϕ_{Ag}.

Final considerations on non-percolating samples.—The analysis of non-percolating samples allowed for the evaluation of material-specific parameters that can be used to help understand the percolating samples.

First of all, the dc conductivity contribution of oxygen transport in Ag is expected to be negligible according to the specific parameters evaluated with impedance spectroscopy. Indeed, the equivalent oxygen conductivity in silver $\sigma_{Ag}(\omega = 0) = 4^2F^2C_OD/(RT)$ is much smaller than the ionic conductivity of ScSZ: for example, at 600°C, $\sigma_{Ag}(\omega = 0) = 1.66 \cdot 10^{-2}$ S m^{-1} while $\sigma_{ScSZ} = 1.786$ S m^{-1}. This means that, in a composite Ag-ScSZ meant for oxygen separation, oxygen is mainly transported via ionic conduction in ScSZ, thus the rate-determining process in the membrane is the conduction of oxygen ions within the ScSZ matrix. This suggests that the lower the silver volume fraction to achieve electronic percolation, the larger the ScSZ volume fraction and so the effective ionic conductivity, thus increasing the oxygen permeation flux (see Eq. 10). Therefore, the fabrication method proposed in this study, which enables for a reduction in the percolation threshold of silver, is a promising approach to minimize the amount of costly metal and simultaneously maximize the effective ionic conductivity and the oxygen permeation flux.

In addition, impedance results indicate that the oxygen reduction reaction at the Ag-ScSZ interface is not rate-determining, thus suggesting silver as a good candidate not only as an electronic conductor but also as a suitable electro-catalyst due to its capability to dissolve oxygen atoms and promote the oxygen reduction at the interface with the ceramic ionic conductor. Therefore, as silver functions as an oxygen reducing agent, the activation of the surface of the Ag-ScSZ percolating membranes is not strictly required.

Conclusions

Composites of silver and scandia stabilized zirconia were prepared according to a coating process using Tollens' reagent, which allows silver to form a percolating network at 8.6 vol %, well below the 30–40 vol% usually considered unavoidable to achieve percolation, reducing the need for costly metal and increasing the oxygen permeation flux. Oxygen was separated from air with a 1 mm thick pellet at 600°C using argon as sweep gas, a value of 0.014 μmol cm^{-2} s^{-1} was obtained without the need for activation of the surface as the silver functions as an oxygen reducing agent.

The impedance response of a non-percolating composite Ag-ScSZ was modelled to provide an insight into the nature of the oxygen reduction and transport in the composites. In addition to estimating the parameters of oxygen diffusion and conductivity in the silver trapped inside the ceramic matrix, the modelling indicated that, although there is migration of atomic oxygen in silver, the main migration path is through the ceramic phase. It also corroborates the conclusion that charge transfer (involved in the reduction of atomic oxygen) at the interface between silver and ScSZ is not a limiting factor for oxygen migration in the composite, suggesting why the membrane is active for oxygen reduction and further surface activation is not strictly required; nonetheless a large surface where oxygen can be incorporated is necessary.

A further challenge for the application of these composites remains the understanding of silver migration under electrochemical gradients as there is evidence of silver mobility under both electric and chemical potentials.

Acknowledgments

A. Bertei has received funding from the European Union's Horizon 2020 research and innovation programme under the Marie Sklodowska-Curie grant agreement no. 654915. A. Maserati acknowledges support from NERC Research Experience Placement. Funding from EPSRC is also acknowledged (EP/M014045/1 and EP/M02346X/1).

Downloaded on 2017-11-09 to IP 155.198.98.217 address. Redistribution subject to ECS terms of use (see ecsdl.org/site/terms_use) unless CC License in place (see abstract).

Appendix

Table AI. All fitted parameters for Ag|ScSZ|Ag. $k_{eff} = 0.5$ is used in the electrode. The electrode thickness is assumed equal to $L_{ed} = 3.2$ μm.

T [°C]	R_1 [Ω m^2]	α	σ_{CPE} [Ω m^2 s$^\alpha$]	p_{ed}	D [m^2 s^{-1}]	C_O [mol m^{-3}]	σ_{ScSZ} [S m^{-1}]
600	$1.07 \cdot 10^{-4}$	−0.737	0.0121	0.467	$9.861 \cdot 10^{-10}$	1.250	1.786
650	$4.99 \cdot 10^{-5}$	−0.755	0.0202	0.456	$3.333 \cdot 10^{-9}$	1.045	3.018
700	$5.03 \cdot 10^{-5}$	−0.717	0.0130	0.476	$4.094 \cdot 10^{-9}$	1.462	4.370
750	$3.81 \cdot 10^{-5}$	−0.705	0.0106	0.501	$8.354 \cdot 10^{-9}$	1.775	5.617
800	$3.15 \cdot 10^{-5}$	−0.761	0.0139	0.574	$1.669 \cdot 10^{-6}$	0.099	6.604

Table AII. All fitted parameters for Ag|Ag-ScSZ|Ag (4.7 vol % Ag). $k_{eff} = 0.5$ is used in the electrode. The electrode thickness is assumed equal to $L_{ed} = 3.2$ μm. This set of parameters shows high consistency with the literature as discussed in the text, thus it must be preferred to the values reported in Table AI.

T [°C]	R_1 [Ω m^2]	α	σ_{CPE} [Ω m^2 s$^\alpha$]	p_{ed}	D [m^2 s^{-1}]	C_O [mol m^{-3}]	ϕ_{Ag}	L_{Ag} [μm]	p_{Ag}
600	$2.57 \cdot 10^{-4}$	−0.486	0.0630	0.375	$6.332 \cdot 10^{-10}$	1.275	0.0710	0.8	0.70
650	$1.03 \cdot 10^{-4}$	−0.617	0.1031	0.357	$9.789 \cdot 10^{-10}$	1.624	0.0473	0.8	0.68
700	$4.25 \cdot 10^{-5}$	−0.746	0.2002	0.345	$1.265 \cdot 10^{-9}$	2.266	0.0473	0.8	0.64
750	$2.10 \cdot 10^{-5}$	−0.816	0.2653	0.369	$1.608 \cdot 10^{-9}$	2.691	0.0473	0.8	0.61

References

1. S. Lucas, *Memoirs of the literary and philosophical society of manchester*, **3**, 376 (1818).
2. W. Eichenauer and G. Mueller, *Zeitschrift fuer Metallkunde*, **53** (1962).
3. R. A. Outlaw, W. K. Peregoy, and B. Hoflund Gar, *Permeation of oxygen through high purity, large grain silver*, in, Technical paper for NASA, Scientific and Technical Information Office.
4. J. Van Herle and A. McEvoy, *J Phys Chem Solids*, **55**, 339 (1994).
5. E. Ruiz-Trejo, P. Boldrin, A. Lubin, F. Tariq, S. Fearn, R. Chater, S. N. Cook, A. Atkinson, R. I. Gruar, C. J. Tighe, J. Darr, and N. P. Brandon, *Chemistry of Materials*, **26**, 3887 (2014).
6. W. Nernst and H. Reynolds, *Nachrichten von der Gesellschaft der Wissenschaften zu Göttingen, Mathematisch-Physikalische Klasse*, **1900**, 328 (1900).
7. C. Wagner, *Naturwissenschaften*, **31**, 265 (1943).
8. T. Mazanec, T. Cable, and R. J. Frye, *Solid State Ionics*, **53**, 111 (1992).
9. Y. Teraoka, H. M. Zhang, S. Furukawa, and N. Yamazoe, *Chem Lett*, 1743 (1985).
10. Z. Shao, W. Yang, Y. Cong, H. Dong, J. Tong, and G. Xiong, *J Membrane Sci*, **172**, 177 (2000).
11. P. Seeharaj and A. Atkinson, *Solid State Ionics*, **204**, 46 (2011).
12. J. Ten Elshof, N. Nguyen, M. Den Otter, and H. Bouwmeester, *J Electrochem Soc*, **144**, 4361 (1997).
13. J. Kim and Y. S. Lin, *J Membrane Sci*, **167**, 123 (2000).
14. W. P. C. Duyvesteyn and G. F. Putnam, *EMC Metals Corporation*, (2014).
15. E. Ruiz-Trejo, P. Boldrin, J. L. Medley-Hallam, J. Darr, A. Atkinson, and N. P. Brandon, *Chem Eng Sci*, **127**, 269 (2015).
16. E. Ruiz-Trejo, Y. N. Zhou, and N. P. Brandon, *Int J Hydrogen Energ*, **40**, 4146 (2015).
17. J. A. Turcaud, H. N. Bez, E. Ruiz-Trejo, C. R. H. Bahl, K. K. Nielsen, A. Smith, and L. F. Cohen, *Acta Mater*, **97**, 413 (2015).
18. E. Ruiz-Trejo, A. Atkinson, and N. P. Brandon, *Journal of Power Sources*, **280**, 81 (2015).
19. Z. Jamil, E. Ruiz-Trejo, P. Boldrin, and N. P. Brandon, *Int J Hydrogen Energ*, **41**(22), 9627 (2016).
20. B. Tollens, *Berichte der deutschen chemischen Gesellschaft*, **15**, 1635 (1882).
21. E. Barsoukov and J. R. Macdonald, *Impedance spectroscopy: theory, experiment, and applications*, John Wiley & Sons (2005).
22. B. Tjaden, S. J. Cooper, D. J. L. Brett, D. Kramer, and P. R. Shearing, *Curr Opin Chem Eng*, **12**, 44 (2016).
23. Y. -W. Zhang, J. -T. Jia, C. -S. Liao, and C. -H. Yan, *J Mater Chem*, **10**, 2137 (2000).
24. C. Haering, A. Roosen, H. Schichl, and M. Schnöller, *Solid State Ionics*, **176**, 261 (2005).
25. M. Angeles-Rosas, M. A. Camacho-López, and E. Ruiz-Trejo, *Solid State Ionics*, **181**, 1349 (2010).
26. J. T. Irvine, J. W. Dobson, T. Politova, S. G. Martín, and A. Shenouda, *Faraday discussions*, **134**, 41 (2007).
27. S. Omar, W. Bin Najib, W. Chen, and N. Bonanos, *J Am Ceram Soc*, **95**, 1965 (2012).
28. *ASM International Handbook Committee, ASM Handbook, Volume 02 - Properties and Selection: Nonferrous Alloys and Special-Purpose Materials*, ASM International (1990).
29. S. J. Krumbein, *Ieee T Compon Hybr*, **11**, 5 (1988).
30. I. P. Mihail, G. M. Vladimir, V. Z. Valentina, P. S. Yuri, and A. L. Andrey, *Journal of Physics D: Applied Physics*, **46**, 045302 (2013).
31. K. Sasaki, M. Muranaka, and T. Terai, *Solid State Ionics*, **181**, 1303 (2010).
32. C. Chatzichristodoulou, W. -S. Park, H. -S. Kim, P. V. Hendriksen, and H. -I. Yoo, *Physical Chemistry Chemical Physics*, **12**, 9637 (2010).
33. J. Sunarso, S. Baumann, J. M. Serra, W. A. Meulenberg, S. Liu, Y. S. Lin, and J. C. D. da Costa, *J Membrane Sci*, **320**, 13 (2008).
34. E. Capoen, M. C. Steil, G. Nowogrocki, M. Malys, C. Pirovano, A. Lofberg, E. Bordes-Richard, J. C. Bolvin, G. Mairesse, and R. N. Vannier, *Solid State Ionics*, **177**, 483 (2006).
35. Z. L. Wu and M. L. Liu, *Solid State Ionics*, **93**, 65 (1996).
36. A. Bertei, J. Pharoah, D. Gawel, and C. Nicolella, *J Electrochem Soc*, **161**, F1243 (2014).
37. A. Bertei, B. Nucci, and C. Nicolella, *Chem Eng Sci*, **101**, 175 (2013).
38. J. M. Zalc, S. C. Reyes, and E. Iglesia, *Chem Eng Sci*, **59**, 2947 (2004).
39. Z. Hashin and S. Shtrikman, *Journal of applied Physics*, **33**, 3125 (1962).
40. C. Chueh, A. Bertei, J. Pharoah, and C. Nicolella, *International Journal of Heat and Mass Transfer*, **71**, 183 (2014).
41. G. Schimmel, J. Sorina-Müller, B. Kempf, and M. Rettenmayr, *Acta Mater*, **58**, 2091 (2010).
42. Y. Arachi, H. Sakai, O. Yamamoto, Y. Takeda, and N. Imanishai, *Solid State Ionics*, **121**, 133 (1999).

Downloaded on 2017-11-09 to IP 155.198.98.217 address. Redistribution subject to ECS terms of use (see ecsdl.org/site/terms_use) unless CC License in place (see abstract).